

# Empowering Time Series Analysis with Large-Scale Multimodal Pretraining

Peng Chen<sup>1</sup> Siyuan Wang<sup>1</sup> Shiyuan Hu<sup>1</sup> Xingjian Wu<sup>1</sup> Yang Shu<sup>1</sup> Zhongwen Rao<sup>2</sup> Meng Wang<sup>2</sup> Yijie Li<sup>2</sup>  
Bin Yang<sup>1</sup> Chenjuan Guo<sup>1</sup>

## Abstract

While existing time series foundation models primarily rely on large-scale unimodal pretraining, they lack complementary modalities to enhance time series understanding. Building multimodal foundation models is a natural next step, but it faces key challenges: 1) lack of a unified multimodal pretraining paradigm and large-scale multimodal corpora for time series analysis; 2) how to effectively integrate heterogeneous modalities and enhance model generalization. To address these challenges, we take an early step toward multimodal foundation models for time series analysis. We first propose a multimodal pretraining paradigm that leverages time series with endogenous modalities (derived images and text) and exogenous knowledge (real-world news), providing a comprehensive multi-view perspective for time series analysis. To support this, we develop an automated data construction pipeline to curate MM-TS, the first large-scale multimodal time series dataset spanning six domains, with up to one billion points. Then we propose HORAI, a frequency-enhanced multimodal foundation model. It integrates two core components: the Frequency-enhanced Cross-Modality Encoder and the Time-Frequency Decoder, designed to effectively fuse multimodal features and enhance model generalization across modalities and domains. After pretraining on MM-TS, HORAI achieves state-of-the-art zero-shot performance on time series forecasting and anomaly detection tasks, demonstrating strong generalization.

## 1. Introduction

Time series analysis is widely applied across diverse domains, including energy management, medical monitoring,

<sup>1</sup>East China Normal University, Shanghai, China <sup>2</sup>HuaWei, ShenZhen, China. Correspondence to: Chenjuan Guo <cjguo@dase.ecnu.edu.cn>.

Preprint. February 6, 2026.

and financial forecasting. Existing time series analysis approaches, ranging from time-series-specific models (Zeng et al., 2023; Nie et al., 2023; Liu et al., 2024b; Chen et al., 2024b) to recent time series foundation models (Woo et al., 2024; Gao et al., 2024; Shi et al., 2025; Anonymous Authors, 2026), primarily rely on time series numerical modality to capture temporal patterns and uncover underlying regularities. While these methods have achieved competitive performance, this single-modality paradigm remains limited in its ability to capture the complex and multifaceted nature of real-world temporal dynamics (Xu et al., 2024a).

At the same time, foundation models in NLP and multimodal learning (Brown et al., 2020; Bai et al., 2023; Wu et al., 2024; Chen et al., 2024c) have shown that large-scale pretraining on massive datasets with complementary modalities can enhance generalization and adaptability across tasks. Inspired by these, we propose developing multimodal foundation models for time series analysis. By incorporating additional modalities for pretraining, such as text and images, the model leverages textual semantics and visual information to better capture complex temporal dynamics and strengthen time series understanding.

However, the development of multimodal foundation models faces several significant challenges. First, the field lacks a multimodal pretraining paradigm and large-scale multimodal corpora for time series analysis. Existing multimodal methods are tailored to specific datasets, lacking a unified pretraining paradigm for broad cross-modal analysis (Jia et al., 2024; Li et al., 2025). Moreover, existing large-scale datasets contain only numerical time series and lack complementary modalities such as text or images, which limits their suitability for multimodal pretraining (Liu et al., 2024c; Woo et al., 2024). Second, the architectural design for integrating different modalities in time series analysis remains underexplored. Each modality exhibits unique characteristics: text provides rich semantic information and offers a holistic, global description of events, whereas images capture localized details and spatial structures (Zhong et al., 2025). Directly fusing time series with textual or visual modalities (Phuong & Lampert, 2019; Kim & Rush, 2016) may result in suboptimal alignment and ineffective representation learning. Therefore, it is critical to design fusion mechanisms that explicitly leverage the unique characteris-

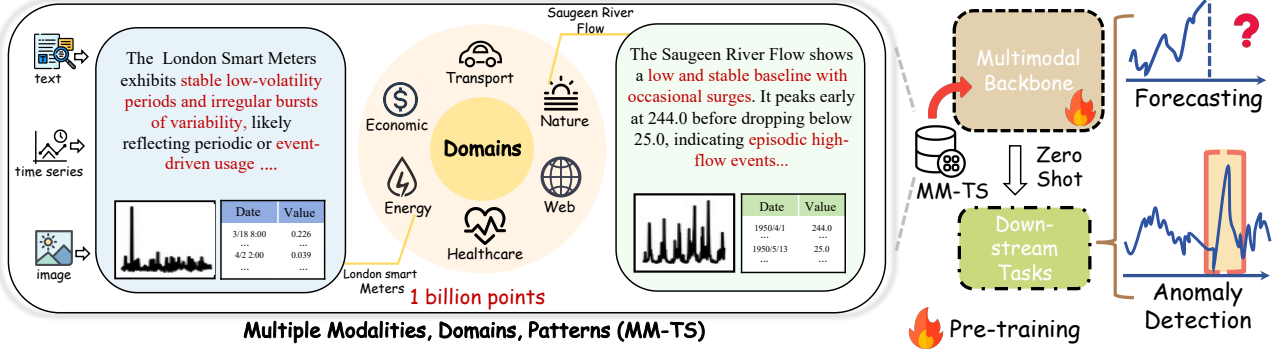


Figure 1. Left: The large-scale multimodal time series dataset MM-TS is characterized by its coverage of various modalities, heterogeneous domains, and diverse temporal patterns. Right: The multimodal foundation model HORAI is pre-trained on the MM-TS dataset and evaluated on downstream scenarios and tasks.

tics of each modality. Third, time series data from different domains exhibit diverse patterns, and the incorporation of multiple modalities further amplifies this diversity. Effectively modeling the heterogeneous patterns across modalities and domains, while enhancing the generalization ability of pretrained models, remains a challenge. Consequently, advancing multi-modal foundation models for time series analysis requires further research and exploration.

In this paper, we take an early step toward developing multimodal foundation models for time series analysis. *On the pretraining paradigm and dataset side*, we propose a multimodal pretraining paradigm that leverages time series with endogenous modalities (derived images and text) and exogenous knowledge (real-world news), providing a comprehensive multi-view perspective for time series analysis. Endogenous modalities capture intrinsic time series characteristics through semantic and visual structures, while exogenous news provides supplementary background context. To support this, we develop an *automated data construction pipeline* that maps raw sequences to visual and textual modalities, aligns them with external news sources, and incorporates multiple LLMs for rigorous quality verification. This process curates MM-TS, the first large-scale multimodal time series dataset. As illustrated in Figure 1, MM-TS integrates three modalities, spanning six diverse domains and a wide range of temporal patterns, with up to one billion points. The three modalities exhibit strong correlations and complementary characteristics, making MM-TS well-suited for multimodal pretraining to learn generalized representations.

*On the modeling side*, we propose **HORAI**, a frequency-enhanced multimodal time series foundation model built on an autoregressive architecture, which consists of two core components: Frequency-enhanced Cross-Modality Encoder and Time-Frequency Decoder. *In the Frequency-enhanced Cross-Modality Encoder*, we leverage the correspondence between modality-specific information and different frequency components of time series to align multiple modal-

ties and enhance time series understanding. Specifically, time series are decomposed into multiple frequency bands, where low-frequency components capture long-term dynamics and align with the global semantics embedded in text, while mid- and high-frequency components encode rapid variations that tend to correspond to the localized patterns present in visual inputs. *In the Time-Frequency Decoder*, we design a Time-Frequency MoE-FFN to learn generalized multimodal representations from multi-domain data. We introduce a time-frequency router that dynamically assigns each token to the suitable expert based on both temporal and frequency features. By incorporating frequency-domain features, the router gains additional cues to better distinguish similar patterns and group them coherently, which enhances feature consistency and improves generalization across domains. Specifically, our contributions are as follows:

- **New Paradigm and Pretraining Datasets:** We propose a multimodal pretraining paradigm that leverages time series along with endogenous modalities (derived images and text) and exogenous knowledge (news), enhancing time series analysis from a comprehensive multi-view perspective. To support this, we develop an automated data construction pipeline to curate MM-TS, the first large-scale multimodal time series dataset.
- **New Model:** We propose HORAI, a frequency-enhanced multimodal foundation model for Time series analysis, which incorporates two core components, the frequency-guided cross-modality encoder and the time-frequency decoder, designed to effectively fuse multimodal features and enhance model generalization across modalities and domains.
- **Comprehensive Evaluation:** After pre-training on large-scale multimodal time series data, HORAI achieves state-of-the-art performance in time series forecasting and anomaly detection across zero-shot inference and few-shot learning situations, which demonstrates strong task versatility and generalization ability.

## 2. Related work

### 2.1. Time Series Analysis

Time series analysis spans a wide range of tasks, including forecasting and anomaly detection (Qiu et al., 2024; Darban et al., 2025; Paparrizos et al., 2022b). Existing approaches can be broadly divided into unimodal and multimodal methods. **Unimodal methods** focus on time series data and employ diverse architectures to model temporal dynamics and channel correlations. These include MLP-based models (Zeng et al., 2023; Xu et al., 2024b), RNN-based models (Flunkert et al., 2017), CNN-based models (Wu et al., 2023; Luo & Wang, 2024), GNN-based models (Zhao et al., 2023; Wu et al., 2021), as well as Transformer-based architectures for capturing long-range dependencies (Zhang & Yan, 2023; Nie et al., 2023; Chen et al., 2024b; Lu et al., 2025). In contrast, **multimodal methods** integrate additional modalities or external knowledge to enhance time series analysis. One line of work introduces endogenous prompts, such as statistical information, channel semantics, or task-related descriptions, to enrich temporal representations (Jin et al., 2024; Chen et al., 2025a; Zhong et al., 2025). Another line of work leverages exogenous textual or visual modalities to provide additional contextual knowledge (Li et al., 2025; Jia et al., 2024; Wang et al., 2025a; Liu et al., 2024a). Although these methods achieve competitive performance, most require retraining and extensive parameter tuning for each dataset, lacking zero-shot inference capabilities. While ChatTime (Wang et al., 2025a) enables direct zero-shot inference, it suffers from precision loss due to data discretization and lacks rich multimodal characterizations. Further comparisons with ChatTime are in Appendix D.

### 2.2. Time Series Foundation Models

Recently, time series foundation models (TSFMs) have attracted increasing attention (Ansari et al., 2024; Das et al., 2024; Goswami et al., 2024; Ekambaram et al., 2024; Chen et al., 2024a; 2025b; Shi et al., 2025; Anonymous Authors, 2026). By pre-training on large-scale time series datasets, these models exhibit strong adaptability to new tasks, enabling both efficient fine-tuning and zero-shot transfer across domains. For instance, Timer (Liu et al., 2024c) employs a decoder-only architecture with autoregressive pre-training to capture temporal dependencies, while MOIRAI (Woo et al., 2024) introduces multi-scale patch projections to model diverse patterns and an any-variate attention mechanism that allows flexible handling of time series with arbitrary dimensionality. ROSE (Wang et al., 2025b) combines frequency decomposition with registers to jointly learn both domain-invariant and domain-specific representations, facilitating knowledge transfer to downstream tasks. Sundial (Liu et al., 2025) proposes a TimeFlow Loss

that predicts the distribution of the next patch, enabling Transformer training supporting probabilistic forecasting.

Existing TSFMs are all pre-trained solely on unimodal time series data, which provides some generalization ability but cannot leverage complementary modalities to model more complex temporal dynamics. In contrast, HORAI effectively leverages multiple modalities through a frequency-enhanced cross-modality encoder and introduces a Time-Frequency Decoder to further strengthen cross-modality and cross-domain generalization during pre-training.

## 3. Methodology

### 3.1. Large-Scale Multimodal Time Series Dataset

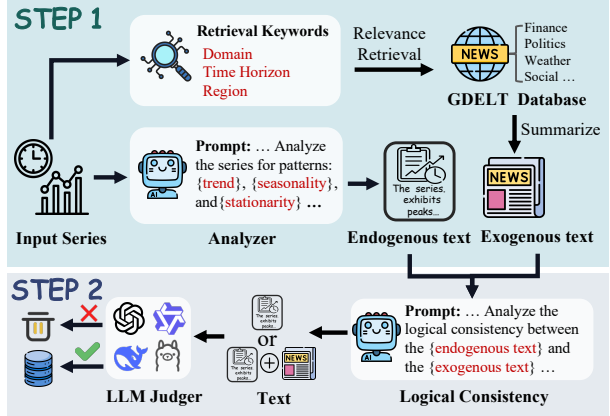


Figure 2. The automated data construction pipeline for multimodal text. It comprises two main stages: 1) Contextual Synthesis, involving endogenous pattern analysis and exogenous news retrieval; and 2) Quality Alignment, which ensures consistency between the synthesized texts and filters low-quality data via an LLM judger.

Large-scale datasets are the cornerstone of pre-training foundation models, enabling them to acquire transferable knowledge and improve generalization across diverse downstream scenarios. However, existing large-scale time series corpora are mostly confined to unimodal time series, which limits the potential of multimodal learning. To address this problem, we conduct MM-TS, the first large-scale multimodal time series dataset for pre-training. As shown in Figure 1, MM-TS integrates three modalities: time series, text, and image, covering six diverse domains, including Energy, Healthcare, Web, Nature, Transport, and Economics. In total, MM-TS contains over 1 billion time points.

For the time series modality, MM-TS spans multiple temporal granularities, including seconds, minutes, hours, and months, and captures diverse characteristics such as periodicity, trends, and non-stationarity (see Appendix A.1 for details). For the visual modality, we construct line-plot images directly from time series, offering an intuitive view of temporal fluctuations and structural patterns.

For the textual modality, to address the scarcity of high-quality, semantically aligned time series and textual pairs, we devise an automated data construction pipeline that uniquely integrates endogenous text with exogenous news. Endogenous text captures the semantic features of time series patterns, and exogenous news provides supplementary background context. Figure 2 shows that the pipeline includes two main stages: Contextual Synthesis and Quality Alignment. In the Contextual Synthesis stage, we adopt a dual-source generation strategy. Given a time series sample, an LLM analyzer GPT-4o first analyzes intrinsic patterns, such as trends and seasonalities, and converts them into structured semantic descriptions as Endogenous text. In parallel, we retrieve and summarize semantically related news events based on keywords from the GDELT Database to serve as Exogenous text. Subsequently, the Quality Alignment stage ensures logical coherence and generation fidelity via two substeps: 1) Logical Consistency Filtering, where GPT-4o discards exogenous news conflicting with endogenous patterns to prevent spurious correlations; and 2) Ensemble Quality Evaluation, where the unified text is scored by multiple LLM judges on plausibility and relevance, retaining only high-confidence text. Further details on the text generation are in the Appendix A.2.

### 3.2. HORAI

To better leverage cross-modal and cross-domain features for time series understanding, we propose HORAI, a frequency-enhanced multimodal foundation model for time series analysis. It consists of two core components: the Frequency-guided Cross-Modality Encoder and the Time-Frequency Decoder. As illustrated in Figure 3, in the Cross-Modality Encoder, the input time series is first decomposed into low-frequency and mid-to-high-frequency components, which are aligned with textual and visual features, respectively. Then, an adaptive modality fusion module combines these aligned representations to produce unified multimodal representations. In the Time-Frequency Decoder, the multimodal representations are first passed into a Time-Frequency MoE-FFN, which is designed to capture diverse patterns across multiple domains. To guide the routing of tokens to appropriate experts, both temporal-domain and frequency-domain features are incorporated. The inclusion of frequency information provides additional cues that help distinguish similar patterns and group them coherently, enhancing the cross-modality and cross-domain generalization. Finally, the representations are projected through a token projection layer for autoregressive pre-training.

#### 3.2.1. FREQUENCY-ENHANCED CROSS-MODAL ENCODER

**Multimodal Embedding.** For notational simplicity, we describe the method using a univariate time series, which

can be easily extended to the multivariate case by treating each channel independently. Given an input time series  $\mathbf{X}_{ts} \in \mathbb{R}^T$ , where  $T$  denotes the sequence length, we first apply instance normalization (Kim et al., 2021) to mitigate distribution shift, resulting in  $\mathbf{X}_{norm} \in \mathbb{R}^T$ .

Since different frequency components capture different aspects of temporal dynamics, with low-frequency components reflecting global trends and mid-to-high-frequency components capturing local variations, we transform the normalized sequence into the frequency domain by the Fast Fourier Transform (FFT), obtaining  $\mathbf{X}_{freq} \in \mathbb{R}^{L/2+1}$ . To separate different frequency bands, we set a ratio parameter  $\alpha$  to define a cutoff threshold  $\tau = \alpha \cdot (L/2 + 1)$ . Based on this threshold, we construct two binary masks:  $\mathbf{M}_{low} \in \{0, 1\}^{L/2+1}$  for low-frequency components and  $\mathbf{M}_{mh} \in \{0, 1\}^{L/2+1}$  for mid-to-high-frequency components. Applying these masks to  $\mathbf{X}_{freq}$  by element-wise multiplication, which are then transformed back into the time domain using the inverse FFT (iFFT). This process produces the low-frequency sequence  $\mathbf{X}_{low} \in \mathbb{R}^L$  and the mid-to-high-frequency sequence  $\mathbf{X}_{mh} \in \mathbb{R}^L$ .

$$\begin{aligned} \mathbf{X}_{low} &= \text{iFFT}(\mathbf{X}_{freq} \odot \mathbf{M}_{mh}), \\ \mathbf{X}_{mh} &= \text{iFFT}(\mathbf{X}_{freq} \odot \mathbf{M}_{low}). \end{aligned} \quad (1)$$

Subsequently, we employ a patching strategy to divide  $\mathbf{X}_{low}$ ,  $\mathbf{X}_{mh}$ , and  $\mathbf{X}_{norm}$  into  $N_{ts}$  patches with patch size  $S$ . These patches are projected and fed into the time-series encoder (Nie et al., 2023), producing corresponding time series representations:  $\mathbf{E}_{low}$ ,  $\mathbf{E}_{mh}$ , and  $\mathbf{E}_{ts} \in \mathbb{R}^{N_{ts} \times D_{ts}}$ .

For the textual input  $\mathbf{X}_{text} \in \mathbb{R}^{L_{text}}$ , we employ a text tokenizer followed by a pre-trained text encoder Qwen-0.5B (Bai et al., 2023) to extract semantic features, yielding  $\mathbf{E}_{text} \in \mathbb{R}^{L_{text} \times D_{text}}$ . For the visual input  $\mathbf{X}_{img}$ , we apply a patching strategy and a pre-trained vision encoder ViT-Base (Dosovitskiy et al., 2021) to obtain image representations  $\mathbf{E}_{img} \in \mathbb{R}^{N_{img} \times D_{img}}$ .

**Frequency-enhanced Cross-Modality Alignment.** Time series often exhibit rich frequency-dependent patterns, where low-frequency components capture global trends and mid-to-high-frequency components reflect local variations. Meanwhile, different modalities contribute differently to these patterns: textual information tends to describe global trends, aligning with low-frequency time series components, whereas visual information focuses more on short-term variation, corresponding to mid-to-high-frequency components (Zhong et al., 2025). Motivated by this, we propose a frequency-enhanced cross-modal fusion that explicitly leverages the characteristic correspondence between modalities and frequency components. Additionally, given the large number of tokens in text and image modalities, we further integrate a Flow-Attention-based alignment mechanism to efficiently model cross-modal interactions.

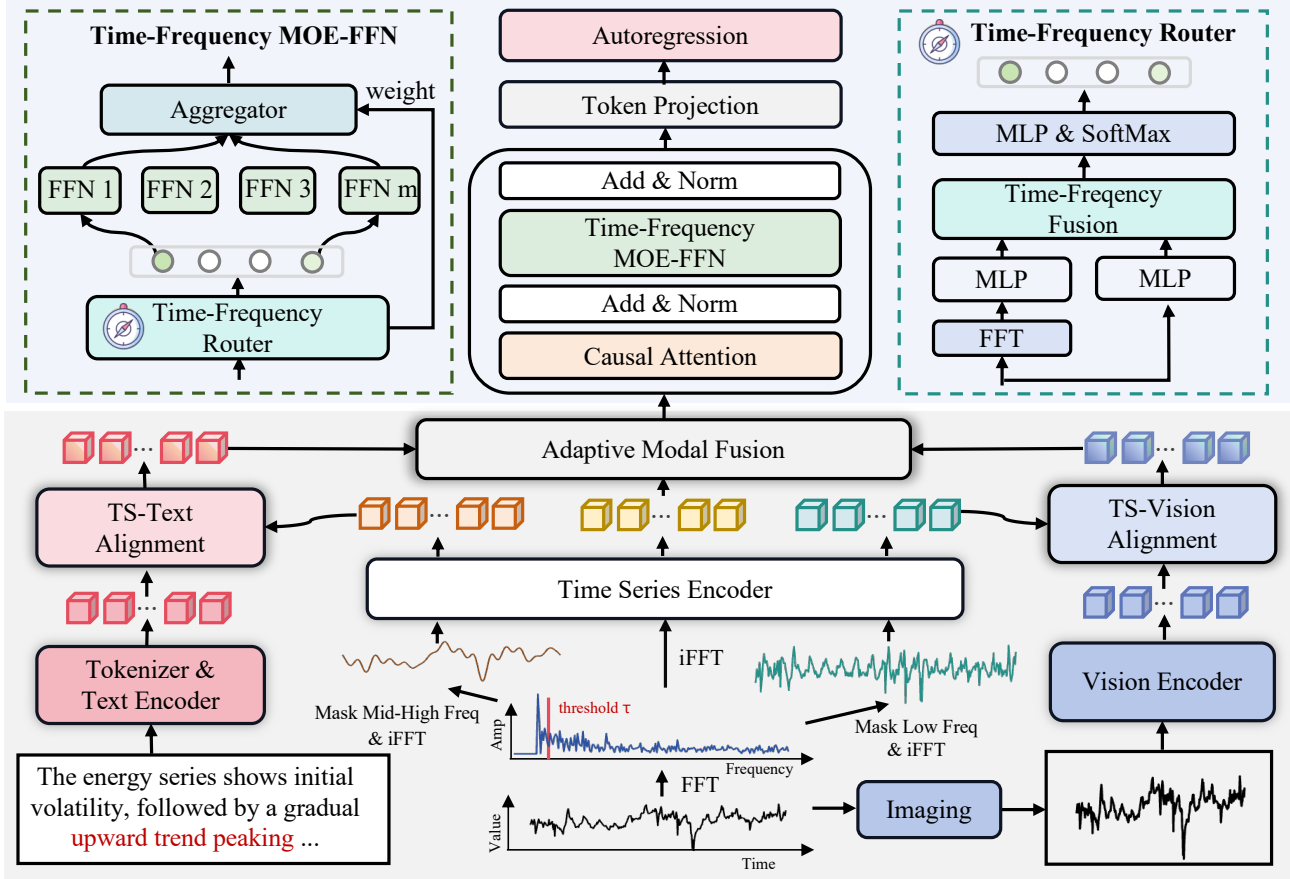


Figure 3. The framework of the proposed HORAI consists of a Frequency-Enhanced Cross-Modal Encoder (gray region) and a Time-Frequency Decoder (blue region).

In the TS-Text Alignment module, the low-frequency time series embeddings and textual embeddings are first projected by MLPs into a shared representation space  $D_{model}$ . Cross-modal fusion is then performed efficiently using the Flow-Attention mechanism (Wu et al., 2022). The core idea is to treat attention as a flow of information and leverage the flow conservation principle to optimize the transmission and aggregation of features across modalities. Specifically, the low-frequency time series embeddings  $\mathbf{E}_{low}$  are mapped to serve as the Query  $\mathbf{Q}$ , while the textual embeddings  $\mathbf{E}'_{text}$  are mapped to serve as the Key  $\mathbf{K}$  and Value  $\mathbf{V}$ . The information flow between tokens is computed as:

$$\begin{aligned} \mathbf{I}_i &= \phi(\mathbf{Q}_i) \sum_{j=1}^{N_{text}} \phi(\mathbf{K}_j)^T, \\ \mathbf{O}_j &= \phi(\mathbf{K}_j) \sum_{i=1}^{N_{ts}} \phi(\mathbf{Q}_i)^T, \hat{\mathbf{O}} = \phi(\mathbf{K}) \sum_{i=1}^{N_{ts}} \frac{\phi(\mathbf{Q}_i)^T}{\mathbf{I}_i}, \quad (2) \\ \mathbf{E}'_{text} &= \frac{\phi(\mathbf{Q})}{\mathbf{I}} (\phi(\mathbf{K})^T (\text{Softmax}(\hat{\mathbf{O}}) \odot \mathbf{V})), \end{aligned}$$

$\phi(\cdot)$  denotes the non-linear projection to the flow space,  $\mathbf{I}_i$  and  $\mathbf{O}_j$  represent the total outgoing and incoming flows for

each token. The output  $\mathbf{E}'_{text}$  is a flow-attention enhanced textual embedding, which has been adaptively aligned with the low-frequency time-series features.

Similar to the low-frequency time-series and text fusion, the TS-Vision Alignment module also leverages the Flow-Attention mechanism to integrate mid-to-high-frequency time-series embeddings  $\mathbf{E}_{mh}$  with image embeddings  $\mathbf{E}_{img}$ , yielding aligned image representations  $\mathbf{E}'_{img} \in \mathbb{R}^{N_{ts} \times D_{model}}$  for subsequent multimodal fusion.

**Adaptive Modal Fusion.** Considering that the contributions of image and text representations vary across different time series patterns, we adaptively fuse the aligned image and text embeddings. The aligned image embeddings  $\mathbf{E}'_{img}$  and text embeddings  $\mathbf{E}'_{text}$  are concatenated along the feature dimension and then passed through a linear projection followed by a sigmoid function  $\sigma$  to perform gated weighting  $\mathbf{G}$ , producing the multimodal representation  $\mathbf{E}_{mm}$ . This representation is subsequently added to the time series embeddings  $\mathbf{E}_{ts}$  to obtain the fused representation  $\mathbf{E}_{fused} \in \mathbb{R}^{N_{ts} \times D_{model}}$ .

$$\mathbf{G} = \sigma(W_g[\mathbf{E}'_{img}, \mathbf{E}'_{text}] + b_g), \quad (3)$$

$$\mathbf{E}_{\text{fused}} = \mathbf{G} \odot \mathbf{E}'_{\text{img}} + (1 - \mathbf{G}) \odot \mathbf{E}'_{\text{text}} + \mathbf{E}_{\text{ts}}. \quad (4)$$

### 3.2.2. TIME-FREQUENCY DECODER

Large-scale time series data inevitably involves diverse domains, which gives rise to a wide variety of temporal patterns (Wang et al., 2025b; Woo et al., 2024). The incorporation of textual and visual modalities further amplifies the diversity. To address this challenge, we propose a Time-Frequency Decoder designed to capture and adapt to different patterns, enhancing the generalization ability of pre-trained models. As illustrated in Figure 3, the Time-Frequency Decoder consists of key components including Causal Attention, Normalization layers, and a Time-Frequency MoE-FFN.

**Time-Frequency MoE-FFN.** Different expert networks can capture distinct patterns from large-scale data, so effectively routing multimodal features to the appropriate experts is crucial. However, relying only on temporal-domain features may lead to entangled representations across different patterns, which makes pattern discrimination less straightforward. By incorporating frequency-domain features, similar patterns can be represented more compactly, offering additional cues for more accurate expert routing. Motivated by this, we propose the Time-Frequency Router, which integrates both temporal and frequency information to enhance the routing process.

Based on the fused multi-modal representation  $\mathbf{E}_{\text{fused}}$ , we obtain representation  $\mathbf{H}$  through causal attention followed by normalization. In the router, each token of  $\mathbf{H}$  is projected in parallel across both temporal and frequency domains: (i) an MLP produces temporal representations  $\mathbf{H}_{\text{temp}}$ , while (ii) an FFT followed by an MLP yields frequency representations  $\mathbf{H}_{\text{freq}}$ . These dual-domain signals are adaptively integrated via a learnable gating function  $G_{\text{router}}$ , resulting in router representation  $\mathbf{H}_r \in \mathbb{R}^{N_{ts} \times D_{model}}$ :

$$\mathbf{H}_r^i = \mathbf{G}_{\text{router}} \odot \text{MLP}(\mathbf{H}^i) + (1 - \mathbf{G}_{\text{router}}) \odot \text{MLP}(\text{FFT}(\mathbf{H}^i)) \quad (5)$$

Given  $\mathbf{H}_r$ , the router applies an MLP-based routing function to compute routing weights  $\mathbf{W} \in \mathbb{R}^M$ , which determine expert assignment. Following a Top-K strategy, the router selects the  $K$  experts with the highest weights, denoting the set of their indexes as  $\mathcal{K}$ . Then their outputs are aggregated through weight-normalized fusion, producing the representation  $\mathbf{H}_{\text{moe}} \in \mathbb{R}^{N_{ts} \times D_{model}}$ :

$$\mathbf{H}_{\text{moe}}^i = \sum_{j \in \mathcal{K}} \frac{\exp(\mathbf{W}_j)}{\sum_{m \in \mathcal{K}} \exp(\mathbf{W}_m)} \text{FFN}_j(\mathbf{H}^i), \quad i = 1, \dots, N_{ts} \quad (6)$$

**Autoregressive Training.** Given the strong performance of the autoregressive paradigm in both NLP (Bai et al., 2023;

Brown et al., 2020) and time series domains (Liu et al., 2025; 2024c), we adopt a GPT-style training objective to predict the next token. This autoregressive formulation not only supports variable input and output lengths flexibly during inference but also excels at iterative, multi-step generation. Specifically, each input token  $\mathbf{X}_i \in \mathbb{R}^S$  is processed through the encoder, decoder, and token projection layer to generate the prediction of the subsequent token  $\hat{\mathbf{X}}_{i+1} \in \mathbb{R}^S$ . The overall optimization objective is defined as:

$$\mathcal{L}_{\text{train}} = \frac{1}{N_{ts}S} \sum_i \|\hat{\mathbf{X}}_i - \mathbf{X}_i\|^2, \quad i = 1, \dots, N_{ts}. \quad (7)$$

## 4. Experiments

### 4.1. Experimental Setup

**Datasets.** We perform pre-training of HORAI on our proposed MM-TS dataset and *ensure no overlap between the pre-training MM-TS dataset and the downstream evaluation datasets*. To assess HORAI’s capability for time series analysis, we use the widely used evaluation datasets (Liu et al., 2024a) for forecasting and anomaly detection tasks. Specific dataset information is in Appendix A.

**Baselines.** We select both time series foundation models and time-series-specific models as baselines. *For the forecasting task*, we select five SOTA foundation models: ChatTime (Wang et al., 2025a), VisionTS (Chen et al., 2024a), ROSE (Wang et al., 2025b), Timer (Liu et al., 2024c), MOIRAI (Woo et al., 2024), and four *multimodal time-series-specific models*: GPT4MTS (Jia et al., 2024), TATS (Li et al., 2025), GPT4TS (Zhou et al., 2023), TimeVLM (Zhong et al., 2025). *For the anomaly detection task*, we select three unimodal foundation models: DADA (Shentu et al., 2025), Timer, UniTS (Gao et al., 2024), and nine time-series-specific models: GPT4TS, LLMixer (Kowsher et al., 2024), TimesNet (Wu et al., 2023), DCdetector (Yang et al., 2023), Anomaly Transformer(A.T.) (Xu et al., 2022), PatchTST (Nie et al., 2023), HBOS (Goldstein & Dengel, 2012), IForest (Liu et al., 2008), and PCA (Shyu et al., 2003).

**Settings.** During pre-training, HORAI is optimized using the Adam optimizer with an initial learning rate of 0.0005 and trained for 20 epochs, employing an early stopping strategy with a patience of 5 epochs. For the forecasting task, all methods predict future values at four horizons to ensure a fair comparison. Additionally, *none of the models employ the drop-last strategy* (Qiu et al., 2024). For the anomaly detection task, evaluation is conducted using three score-based metrics: AUC-ROC, VUS-ROC, and VUS-PR (Paparizos et al., 2022a), which are threshold-independent. Notably, **time series foundation models perform zero-shot inference directly, whereas time-series-specific models are trained in a full-shot setting for comparison**.

Table 1. Time series forecasting results under zero-shot and full-shot settings, reported as the average across four prediction horizons. The best results are highlighted in **bold**, and the second-best results are underlined. Full results are presented in the Table 10.

Type	⌚ Time Series Foundation Models (Zero-Shot)												⌚ Time-Series-Specific Models (Full-Shot)							
	HORAI		ChatTime		VisionTS		ROSE		Timer		MOIRAI		GPT4MTS		TATS		GPT4TS		TimeVLM	
Models	MSE	MAE	MSE	MAE	MSE	MAE	MSE	MAE	MSE	MAE	MSE	MAE	MSE	MAE	MSE	MAE	MSE	MAE	MSE	MAE
<b>Agriculture</b>	<b>0.201</b>	0.309	0.369	0.410	0.290	0.336	0.345	0.372	0.289	0.339	0.272	0.403	0.225	<u>0.298</u>	<u>0.215</u>	0.301	0.220	<b>0.294</b>	0.237	0.302
<b>Climate</b>	<b>0.857</b>	<b>0.734</b>	1.860	1.106	1.307	0.930	1.475	0.987	<u>0.888</u>	<u>0.764</u>	1.921	1.095	1.182	0.889	1.180	0.887	1.184	0.891	1.195	0.899
<b>Energy</b>	<b>0.208</b>	<b>0.325</b>	<u>0.247</u>	<u>0.352</u>	0.304	0.420	0.386	0.479	0.274	0.359	0.324	0.417	0.262	0.380	0.255	0.368	0.260	0.376	0.260	0.374
<b>Environment</b>	<b>0.309</b>	<b>0.393</b>	0.359	0.456	0.354	0.436	0.392	0.456	0.351	0.428	0.351	0.403	0.323	0.400	0.319	0.396	0.322	<u>0.393</u>	<u>0.319</u>	0.397
<b>Social Good</b>	<b>0.819</b>	0.497	1.069	0.503	1.126	0.618	1.141	0.581	0.974	0.489	1.430	0.651	0.920	0.451	0.918	<b>0.428</b>	0.917	0.476	<u>0.868</u>	<u>0.444</u>
<b>Traffic</b>	<b>0.165</b>	<u>0.244</u>	0.596	0.610	0.281	0.407	0.341	0.451	0.188	0.290	0.406	0.468	0.203	0.261	<u>0.179</u>	<b>0.238</b>	0.206	0.266	0.216	0.319
<b>EWJ</b>	<b>0.589</b>	<b>0.543</b>	0.887	0.641	0.645	0.584	0.706	0.605	0.696	0.595	0.937	0.688	0.626	0.549	0.612	0.546	<u>0.607</u>	<u>0.543</u>	0.609	0.544
<b>KR</b>	<b>0.551</b>	<b>0.448</b>	0.565	0.455	0.671	0.522	0.555	0.480	0.549	0.463	0.992	0.629	0.555	<u>0.450</u>	0.578	0.449	0.578	0.448	0.584	0.454
<b>MDT</b>	<b>0.376</b>	<b>0.434</b>	0.496	0.479	0.433	0.485	0.461	0.493	0.389	0.448	0.606	0.569	0.385	0.442	0.389	<u>0.436</u>	0.391	0.438	0.392	0.437
<b>1<sup>st</sup> Count</b>	<b>9</b>	6	0	0	0	0	0	0	0	0	0	0	0	0	0	2	0	1	0	0

## 4.2. Time Series Forecasting

As shown in Table 1, HORAI achieves state-of-the-art forecasting performance compared to both unimodal foundation models and multimodal time-series-specific models, achieving top performance on 15 out of 18 cases. Specifically, relative to unimodal foundation models, HORAI outperforms ROSE with reductions of 29.6% in MSE. These results indicate that HORAI effectively leverages multimodal information to enhance time series understanding and improve predictive accuracy. Compared to multimodal time-series-specific models trained in a full-shot manner, HORAI achieves superior performance even in the zero-shot setting: exceeding GPT4MTS by 11.4% in MSE, and surpassing TimeVLM by 12.0% in MSE. This demonstrates that pre-training on the large-scale multimodal time series dataset equips HORAI with strong generalization ability.

## 4.3. Time Series Anomaly Detection

As illustrated in Table 2, HORAI achieves state-of-the-art anomaly detection performance compared to both unimodal foundation models and time-series-specific models, attaining top results on 13 out of 15 cases. Compared to DADA, a general time series anomaly detector, HORAI outperforms it by 13.4%, 19.5%, and 19.2% in AUC-ROC, VUS-ROC, and VUS-PR, respectively, under the zero-shot setting. This highlights that integrating multimodal data, such as text and images, enables the model to identify anomalous patterns better. Against time-series-specific models, HORAI outperforms GPT4TS by 12.2%, 20.2%, and 22.6% in AUC-ROC, VUS-ROC, and VUS-PR. These results demonstrate that pre-training on large-scale, multi-domain data equips HORAI with general detection capability, effectively distinguishing between diverse normal and anomalous patterns.

## 4.4. Ablation Study

To evaluate the effectiveness of each component in HORAI, we conduct ablation experiments. Figure 4 illustrates the

unique impact of each module. Removing the image and text modalities (W/O Modality) leads to a drop in performance, demonstrating that HORAI effectively leverages textual semantics and visual spatial information to enhance time series modeling. In the Modality Exchange variant, mid- and high-frequency time series features are aligned with texts, while low-frequency features are aligned with images. In contrast, HORAI aligns low-frequency features with text and mid- to high-frequency features with images, effectively exploiting the correspondence between modality-specific information and different frequency components of the time series, which improves modeling performance. This demonstrates that frequency-aware cross-modality alignment is crucial for capturing complementary patterns across modalities. Replacing the Time-Frequency MoE-FFN with a standard FFN (W/O MoE-FFN) shows that the MoE-FFN allows each expert to capture distinct patterns, thereby enhancing the model’s generalization ability. Removing frequency information from the router (W/O Router) demonstrates that incorporating frequency information helps guide multimodal tokens to the most appropriate FFN experts, further improving performance.

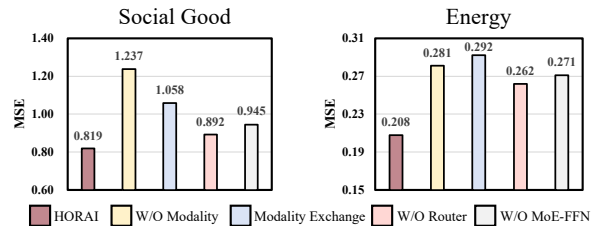


Figure 4. Ablation study on the Social Good dataset and the Energy dataset.

## 4.5. Model Analysis

Due to the limitation of space, we provide the sensitivity analysis, analysis of specific modalities and alignment strategies, and experiments on replacing different text and vision encoders in Appendices E.1, E.2, and E.3, respectively.

Table 2. Time series anomaly detection results under zero-shot and full-shot settings. The best results are in **bold**, and the second-best results are underlined. More metric results are in Table 11.

Type	Metric	Time Series Foundation Models (Zero-Shot)					Time-Series-Specific Models (Full-Shot)							
		HORAI	DADA	Timer	UniTS	GPT4TS	LLMMixer	TimesNet	DCdetector	A.T.	PatchTST	HBOS	IForest	PCA
EWJ	AUC_ROC	<b>86.95</b>	79.11	76.15	79.87	75.58	57.69	<u>82.39</u>	53.40	43.81	78.53	71.82	69.20	54.35
	VUS_ROC	<b>82.78</b>	71.79	67.72	73.91	67.95	52.79	<u>75.76</u>	47.10	31.75	71.96	62.07	59.24	45.26
	VUS_PR	<b>48.27</b>	43.36	33.17	39.32	35.63	15.13	<u>43.15</u>	15.37	10.85	36.08	41.19	37.81	19.38
MDT	AUC_ROC	<b>91.22</b>	79.04	75.65	73.19	74.79	60.30	<u>86.67</u>	53.82	56.44	84.55	60.26	63.92	54.51
	VUS_ROC	<b>86.82</b>	66.76	60.28	58.67	62.30	46.80	<u>83.40</u>	45.02	44.53	77.69	55.30	54.02	44.09
	VUS_PR	<b>56.88</b>	46.81	38.38	37.61	44.81	15.21	<u>52.13</u>	15.72	15.93	41.67	44.77	35.32	22.93
KR	AUC_ROC	<b>96.38</b>	79.53	66.72	80.95	78.30	65.77	<u>85.88</u>	52.97	51.25	82.15	75.16	74.45	63.58
	VUS_ROC	<b>93.54</b>	70.82	75.99	73.93	67.81	47.06	<u>79.00</u>	43.04	41.97	74.65	58.77	60.70	47.51
	VUS_PR	<b>60.76</b>	45.90	51.41	43.32	38.23	19.10	<u>51.60</u>	8.49	7.94	36.18	54.17	43.31	24.19
Energy	AUC_ROC	<b>68.44</b>	62.33	60.54	63.38	66.54	61.31	<u>68.36</u>	48.75	38.68	66.70	60.80	60.32	61.14
	VUS_ROC	<b>62.42</b>	54.37	46.03	51.15	53.10	53.04	<u>59.47</u>	45.93	31.56	58.31	51.50	53.61	53.07
	VUS_PR	35.24	34.18	29.46	31.04	31.68	30.35	38.61	22.57	19.69	34.41	<u>42.57</u>	<b>46.03</b>	44.30
Weather	AUC_ROC	<b>81.49</b>	66.37	80.86	81.22	74.47	79.60	<u>81.10</u>	47.90	47.11	82.02	64.47	67.81	67.71
	VUS_ROC	<b>80.40</b>	61.03	73.22	75.08	70.03	71.71	<b>81.91</b>	45.56	43.32	79.97	54.16	56.45	57.38
	VUS_PR	<b>50.76</b>	30.00	43.21	44.35	41.30	43.47	50.09	18.33	19.17	<u>50.13</u>	46.58	49.66	47.13
1 <sup>st</sup> Count		13	0	0	0	0	0	1	0	0	0	0	1	0

**Fine-tune with downstream data.** To examine how the amount of fine-tuning data affects downstream performance, we evaluate HORAI by progressively enlarging the training portion of the Environment dataset. As shown in Figure 5 (a), the forecasting accuracy steadily improves as more data is used, reaching its best with the full dataset. Specifically, the MAE decreases from 0.393 to 0.370, and the MSE decreases from 0.309 to 0.259. These results highlight HORAI’s strong adaptability to downstream data availability.

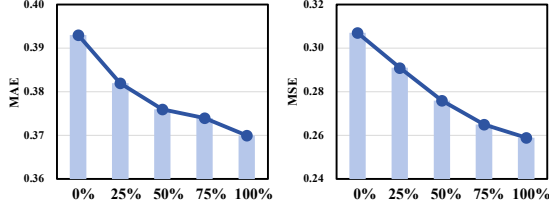


Figure 5. Fine-tuning HORAI with different data percentages on the Environment dataset.

**Text Replacement.** To examine whether HORAI genuinely leverages semantic information from two types of text, we conduct a series of text replacement experiments with four variants: randomly generated unrelated text (Random Text), exogenous text only (Exogenous Text), endogenous text only (Endogenous Text), and removing the entire text modality (W/O Text). As shown in Figure 6, the full HORAI model consistently achieves the lowest MSE across both datasets, demonstrating the synergistic benefit of integrating endogenous descriptions with exogenous real-world news. Notably, utilizing either Exogenous Text or Endogenous Text independently yields better performance than W/O Text, confirming that both distinct sources provide

valuable information. Introducing random text leads to a substantial performance drop, even worse than removing the text modality on the EWJ dataset, indicating that HORAI does not simply rely on the presence of text but actually understands and exploits its semantic content.

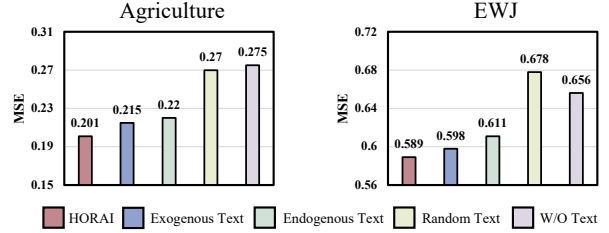


Figure 6. Text replacement experiments on the Agriculture dataset and the EWJ dataset.

## 5. Conclusion

In this paper, we first propose a multimodal pretraining paradigm that leverages time series with endogenous images and text and exogenous news, providing a comprehensive multi-view perspective for time series analysis. To support this, we develop an automated data construction pipeline to curate MM-TS, the first large-scale multimodal time series dataset spanning six domains. Then we propose HORAI, a frequency-enhanced multimodal foundation model. It integrates two core components: the Frequency-guided Cross-Modality Encoder and the Time-Frequency Decoder, effectively fusing different multimodal features and enhancing model generalization. After pre-training on MM-TS, HORAI achieves SOTA performance in time series forecasting and anomaly detection tasks, which demonstrates strong task versatility and generalization ability.

## References

Alexandrov, A., Benidis, K., Bohlke-Schneider, M., Flunkert, V., Gasthaus, J., Januschowski, T., Maddix, D. C., Rangapuram, S. S., Salinas, D., Schulz, J., Stella, L., Türkmen, A. C., and Wang, Y. Gluonts: Probabilistic and neural time series modeling in python. *J. Mach. Learn. Res.*, 21:116:1–116:6, 2020.

Anonymous Authors. Flame: Flow enhanced legendre memory models for general time series forecasting. Concurrent Submission to ICML, 2026. Filename: flame\_ICML\_2026.pdf.

Ansari, A. F., Stella, L., Türkmen, A. C., Zhang, X., Mercado, P., Shen, H., Shchur, O., Rangapuram, S. S., Pineda-Arango, S., Kapoor, S., Zschiegner, J., Maddix, D. C., Mahoney, M. W., Torkkola, K., Wilson, A. G., Bohlke-Schneider, M., and Wang, Y. Chronos: Learning the language of time series. *CoRR*, abs/2403.07815, 2024.

Bagnall, A., Dau, H. A., Lines, J., Flynn, M., Large, J., Bostrom, A., Southam, P., and Keogh, E. The uea multivariate time series classification archive, 2018. *arXiv preprint arXiv:1811.00075*, 2018.

Bai, J., Bai, S., Chu, Y., Cui, Z., Dang, K., Deng, X., Fan, Y., Ge, W., Han, Y., Huang, F., et al. Qwen technical report. *arXiv preprint arXiv:2309.16609*, 2023.

Brown, T. B., Mann, B., Ryder, N., Subbiah, M., Kaplan, J., Dhariwal, P., Neelakantan, A., Shyam, P., Sastry, G., Askell, A., Agarwal, S., Herbert-Voss, A., Krueger, G., Henighan, T., Child, R., Ramesh, A., Ziegler, D. M., Wu, J., Winter, C., Hesse, C., Chen, M., Sigler, E., Litwin, M., Gray, S., Chess, B., Clark, J., Berner, C., McCandlish, S., Radford, A., Sutskever, I., and Amodei, D. Language models are few-shot learners. In *NeurIPS*, 2020.

Chen, M., Shen, L., Li, Z., Wang, X. J., Sun, J., and Liu, C. Visions: Visual masked autoencoders are free-lunch zero-shot time series forecasters. *arXiv preprint arXiv:2408.17253*, 2024a.

Chen, P., Zhang, Y., Cheng, Y., Shu, Y., Wang, Y., Wen, Q., Yang, B., and Guo, C. Pathformer: Multi-scale transformers with adaptive pathways for time series forecasting. In *ICLR*, 2024b.

Chen, P., Wang, Y., Shu, Y., Cheng, Y., Zhao, K., Rao, Z., Pan, L., Yang, B., and Guo, C. Cc-time: Cross-model and cross-modality time series forecasting. *arXiv preprint arXiv:2508.12235*, 2025a.

Chen, Y., Huang, S., Cheng, Y., Chen, P., Rao, Z., Shu, Y., Yang, B., Pan, L., and Guo, C. Aimts: Augmented series and image contrastive learning for time series classification. *arXiv preprint arXiv:2504.09993*, 2025b.

Chen, Z., Wu, J., Wang, W., Su, W., Chen, G., Xing, S., Zhong, M., Zhang, Q., Zhu, X., Lu, L., et al. Internvl: Scaling up vision foundation models and aligning for generic visual-linguistic tasks. In *CVPR*, pp. 24185–24198, 2024c.

Darban, Z. Z., Webb, G. I., Pan, S., Aggarwal, C., and Salehi, M. Deep learning for time series anomaly detection: A survey. *ACM Comput. Surv.*, 57(1):15:1–15:42, 2025.

Das, A., Kong, W., Sen, R., and Zhou, Y. A decoder-only foundation model for time-series forecasting. In *ICML*, 2024.

Dau, H. A., Bagnall, A., Kamgar, K., Yeh, C.-C. M., Zhu, Y., Gharghabi, S., Ratanamahatana, C. A., and Keogh, E. The ucr time series archive. *IEEE/CAA Journal of Automatica Sinica*, 6(6):1293–1305, 2019.

Dong, Z., Fan, X., and Peng, Z. FNSPID: A comprehensive financial news dataset in time series. In Baeza-Yates, R. and Bonchi, F. (eds.), *SIGKDD*, pp. 4918–4927, 2024.

Dosovitskiy, A., Beyer, L., Kolesnikov, A., Weissenborn, D., Zhai, X., Unterthiner, T., Dehghani, M., Minderer, M., Heigold, G., Gelly, S., Uszkoreit, J., and Houlsby, N. An image is worth 16x16 words: Transformers for image recognition at scale. In *ICLR*, 2021.

Ekambaram, V., Jati, A., Dayama, P., Mukherjee, S., Nguyen, N., Gifford, W. M., Reddy, C., and Kalagnanam, J. Tiny time mixers (ttms): Fast pre-trained models for enhanced zero/few-shot forecasting of multivariate time series. In *NeurIPS*, 2024.

Flunkert, V., Salinas, D., and Gasthaus, J. Deepar: Probabilistic forecasting with autoregressive recurrent networks. *CoRR*, abs/1704.04110, 2017.

Gao, S., Koker, T., Queen, O., Hartvigsen, T., Tsilgkardis, T., and Zitnik, M. Units: A unified multi-task time series model. In *NeurIPS*, 2024.

Godahewa, R., Bergmeir, C., Webb, G. I., Hyndman, R. J., and Montero-Manso, P. Monash time series forecasting archive. *arXiv preprint arXiv:2105.06643*, 2021.

Goldstein, M. and Dengel, A. Histogram-based outlier score (hbos): A fast unsupervised anomaly detection algorithm. *KI-2012: poster and demo track*, 1:59–63, 2012.

Goswami, M., Szafer, K., Choudhry, A., Cai, Y., Li, S., and Dubrawski, A. MOMENT: A family of open time-series foundation models. In *ICML*, 2024.

Jia, F., Wang, K., Zheng, Y., Cao, D., and Liu, Y. Gpt4mts: Prompt-based large language model for multimodal time-series forecasting. In *AAAI*, volume 38, pp. 23343–23351, 2024.

Jin, M., Wang, S., Ma, L., Chu, Z., Zhang, J. Y., Shi, X., Chen, P., Liang, Y., Li, Y., Pan, S., and Wen, Q. Time-llm: Time series forecasting by reprogramming large language models. In *ICLR*, 2024.

Kim, T., Kim, J., Tae, Y., Park, C., Choi, J.-H., and Choo, J. Reversible instance normalization for accurate time-series forecasting against distribution shift. In *ICLR*, 2021.

Kim, Y. and Rush, A. M. Sequence-level knowledge distillation. *CoRR*, abs/1606.07947, 2016.

Kowsher, M., Sobuj, M. S. I., Prrottasha, N. J., Alanis, E. A., Garibay, O. O., and Yousefi, N. Llm-mixer: Multiscale mixing in llms for time series forecasting. *arXiv preprint arXiv:2410.11674*, 2024.

Li, Z., Lin, X., Liu, Z., Zou, J., Wu, Z., Zheng, L., Fu, D., Zhu, Y., Hamann, H., Tong, H., et al. Language in the flow of time: Time-series-paired texts weaved into a unified temporal narrative. *arXiv preprint arXiv:2502.08942*, 2025.

Liu, F. T., Ting, K. M., and Zhou, Z.-H. Isolation forest. In *ICDM*, pp. 413–422, 2008.

Liu, H., Xu, S., Zhao, Z., Kong, L., Prabhakar Kamarthi, H., Sasanur, A., Sharma, M., Cui, J., Wen, Q., Zhang, C., et al. Time-mmd: Multi-domain multimodal dataset for time series analysis. *NeurIPS*, 37:77888–77933, 2024a.

Liu, M., Zeng, A., Chen, M., Xu, Z., Lai, Q., Ma, L., and Xu, Q. Scinet: Time series modeling and forecasting with sample convolution and interaction. *NeurIPS*, 35: 5816–5828, 2022.

Liu, Y., Hu, T., Zhang, H., Wu, H., Wang, S., Ma, L., and Long, M. itransformer: Inverted transformers are effective for time series forecasting. In *ICLR*, 2024b.

Liu, Y., Zhang, H., Li, C., Huang, X., Wang, J., and Long, M. Timer: Generative pre-trained transformers are large time series models. In *ICML*, 2024c.

Liu, Y., Qin, G., Shi, Z., Chen, Z., Yang, C., Huang, X., Wang, J., and Long, M. Sundial: A family of highly capable time series foundation models. *CoRR*, abs/2502.00816, 2025.

Lu, J., Chen, P., Guo, C., Shu, Y., Wang, M., and Yang, B. Towards non-stationary time series forecasting with temporal stabilization and frequency differencing. *arXiv preprint arXiv:2511.08229*, 2025.

Luo, D. and Wang, X. Moderntcn: A modern pure convolution structure for general time series analysis. In *ICLR*, 2024.

McCracken, M. W. and Ng, S. Fred-md: A monthly database for macroeconomic research. *Journal of Business & Economic Statistics*, 34(4):574–589, 2016.

Nie, Y., Nguyen, N. H., Sinthong, P., and Kalagnanam, J. A time series is worth 64 words: Long-term forecasting with transformers. In *ICLR*, 2023.

Paparrizos, J., Boniol, P., Palpanas, T., Tsay, R. S., Elmore, A., and Franklin, M. J. Volume under the surface: a new accuracy evaluation measure for time-series anomaly detection. *Proceedings of the VLDB Endowment*, 15(11): 2774–2787, 2022a.

Paparrizos, J., Kang, Y., Boniol, P., Tsay, R. S., Palpanas, T., and Franklin, M. J. Tsb-uad: an end-to-end benchmark suite for univariate time-series anomaly detection. *VLDB*, 15(8):1697–1711, 2022b.

Phuong, M. and Lampert, C. Towards understanding knowledge distillation. In Chaudhuri, K. and Salakhutdinov, R. (eds.), *ICML*, volume 97, pp. 5142–5151, 2019.

Qiu, X., Hu, J., Zhou, L., Wu, X., Du, J., Zhang, B., Guo, C., Zhou, A., Jensen, C. S., Sheng, Z., and Yang, B. TFB: towards comprehensive and fair benchmarking of time series forecasting methods. *Proc. VLDB Endow.*, 17(9): 2363–2377, 2024.

Shentu, Q., Li, B., Zhao, K., Shu, Y., Rao, Z., Pan, L., Yang, B., and Guo, C. Towards a general time series anomaly detector with adaptive bottlenecks and dual adversarial decoders. In *ICLR*, 2025.

Shi, X., Wang, S., Nie, Y., Li, D., Ye, Z., Wen, Q., and Jin, M. Time-moe: Billion-scale time series foundation models with mixture of experts. In *ICLR*, 2025.

Shyu, M.-L., Chen, S.-C., Sarinnapakorn, K., and Chang, L. A novel anomaly detection scheme based on principal component classifier. 2003.

Taieb, S. B., Bontempi, G., Atiya, A. F., and Sorjamaa, A. A review and comparison of strategies for multi-step ahead time series forecasting based on the nn5 forecasting competition. *Expert systems with applications*, 39(8): 7067–7083, 2012.

Wang, C., Qi, Q., Wang, J., Sun, H., Zhuang, Z., Wu, J., Zhang, L., and Liao, J. Chattime: A unified multimodal time series foundation model bridging numerical and textual data. In *AAAI*, pp. 12694–12702, 2025a.

Wang, J., Jiang, J., Jiang, W., Han, C., and Zhao, W. X. Towards efficient and comprehensive urban spatial-temporal prediction: A unified library and performance benchmark. *CoRR*, abs/2304.14343, 2023.

Wang, Y., Han, Y., Wang, H., and Zhang, X. Contrast everything: A hierarchical contrastive framework for medical time-series. *NeurIPS*, 36, 2024.

Wang, Y., Qiu, Y., Chen, P., Zhao, K., Shu, Y., Rao, Z., Pan, L., Yang, B., and Guo, C. Towards a general time series forecasting model with unified representation and adaptive transfer. In *ICML*, 2025b.

Woo, G., Liu, C., Kumar, A., Xiong, C., Savarese, S., and Sahoo, D. Unified training of universal time series forecasting transformers. In *ICML*, 2024.

Wu, H., Wu, J., Xu, J., Wang, J., and Long, M. Flowformer: Linearizing transformers with conservation flows. *arXiv preprint arXiv:2202.06258*, 2022.

Wu, H., Hu, T., Liu, Y., Zhou, H., Wang, J., and Long, M. Timesnet: Temporal 2d-variation modeling for general time series analysis. In *ICLR*, 2023.

Wu, S., Fei, H., Qu, L., Ji, W., and Chua, T. Next-gpt: Any-to-any multimodal LLM. In *ICML*, 2024.

Wu, X., Zhang, D., Guo, C., He, C., Yang, B., and Jensen, C. S. Autocts: Automated correlated time series forecasting. *VLDB*, 15(4):971–983, 2021.

Xu, J., Wu, H., Wang, J., and Long, M. Anomaly transformer: Time series anomaly detection with association discrepancy. In *ICLR*, 2022.

Xu, Z., Wang, H., and Xu, Q. Intervention-aware forecasting: Breaking historical limits from a system perspective. *arXiv preprint arXiv:2405.13522*, 2024a.

Xu, Z., Zeng, A., and Xu, Q. FITS: modeling time series with 10k parameters. In *ICLR*, 2024b.

Yang, Y., Zhang, C., Zhou, T., Wen, Q., and Sun, L. Dcdetector: Dual attention contrastive representation learning for time series anomaly detection. In *SIGKDD*, pp. 3033–3045, 2023.

Zeng, A., Chen, M., Zhang, L., and Xu, Q. Are transformers effective for time series forecasting? In *AAAI*, pp. 11121–11128, 2023.

Zhang, S., Guo, B., Dong, A., He, J., Xu, Z., and Chen, S. X. Cautionary tales on air-quality improvement in beijing. *Proceedings of the Royal Society A: Mathematical, Physical and Engineering Sciences*, 473(2205):20170457, 2017.

Zhang, Y. and Yan, J. Crossformer: Transformer utilizing cross-dimension dependency for multivariate time series forecasting. In *ICLR*, 2023.

Zhao, K., Guo, C., Cheng, Y., Han, P., Zhang, M., and Yang, B. Multiple time series forecasting with dynamic graph modeling. *Proc. VLDB Endow.*, 17(4):753–765, 2023.

Zhong, S., Ruan, W., Jin, M., Li, H., Wen, Q., and Liang, Y. Time-vlm: Exploring multimodal vision-language models for augmented time series forecasting. In *ICML*, 2025.

Zhou, T., Niu, P., Wang, X., Sun, L., and Jin, R. One fits all: Power general time series analysis by pretrained LM. In *NeurIPS*, 2023.

## A. Datasets

### A.1. Pre-train Dataset MM-TS of Time Series Modality

For time series modality, we assemble a large and diverse set of publicly available time series datasets covering domains such as energy, nature, transportation, web, health, and economics. The corpus contains around 1 billion time points, with a strict separation from all target evaluation datasets. The datasets vary widely in their sampling frequencies—from millisecond-level measurements to monthly observations—reflecting both the heterogeneity of real-world scenarios and the complexity of temporal dynamics.

Table 3. List of pretraining datasets of time series modality.

Domain	Dataset	Frequency	Time Pionts	Source
Energy	Aus. Electricity Demand	Half Hourly	1155264	Monash (Godahewa et al., 2021)
	Wind	4 Seconds	7397147	Monash (Godahewa et al., 2021)
	Wind Farms	Minutely	172178060	Monash (Godahewa et al., 2021)
	Solar Power	4 Seconds	7397222	Monash (Godahewa et al., 2021)
	London Smart Meters	Half Hourly	166527216	Monash (Godahewa et al., 2021)
	BDG-2 Rat	Hourly	4596080	(Alexandrov et al., 2020)
	BDG-2 Panther	Hourly	893840	(Alexandrov et al., 2020)
	BDG-2 Fox	Hourly	2285288	(Alexandrov et al., 2020)
Nature	Phoneme	-	2160640	UCR(Dau et al., 2019)
	PRSA	Hourly	4628448	(Zhang et al., 2017)
	Temperature Rain	Daily	23252200	Monash (Godahewa et al., 2021)
	StarLightCurves	-	9457664	UCR (Dau et al., 2019)
	Worms	0.033 Seconds	232200	UCR (Dau et al., 2019)
	Saugeen River Flow	Daily	23741	Monash (Godahewa et al., 2021)
	Sunspot	Daily	73924	Monash (Godahewa et al., 2021)
	Weather	Daily	43032000	Monash (Godahewa et al., 2021)
	KDD Cup 2018	Daily	2942364	Monash(Godahewa et al., 2021)
	US Births	Daily	7305	Monash (Godahewa et al., 2021)
Healthcare	MotorImagery	0.001 Seconds	72576000	UEA (Bagnall et al., 2018)
	AtrialFibrillation	0.008 Seconds	38400	UEA (Bagnall et al., 2018)
	PigArtPressure	-	624000	UCR (Dau et al., 2019)
	TDbrain	0.002 Seconds	79232703	(Wang et al., 2024)
Transport	Pems03	5 Minute	9382464	(Liu et al., 2022)
	Pems08	5 Minute	3035520	(Liu et al., 2022)
	Pems-bay	5 Minute	16937700	(Liu et al., 2022)
	Pedestrian_Counts	Hourly	3132346	Monash (Godahewa et al., 2021)
	SZ-Taxi	15 Minute	464256	(Wang et al., 2023)
	Taxi	Half Hourly	40584636	(Alexandrov et al., 2020)
Web	Uber TLC	Hourly	510284	(Alexandrov et al., 2020)
	Web Traffic	Daily	116485589	Monash (Godahewa et al., 2021)
Economic	FRED.MD	Monthly	77896	(McCracken & Ng, 2016)
	Bitcoin	Daily	75364	Monash (Godahewa et al., 2021)
	NN5	Daily	87801	(Taieb et al., 2012)

## A.2. Pre-train Dataset MM-TS of Text Modality

To address the scarcity of high-quality, semantically aligned time series and text pairs, we design a two-stage automated data construction pipeline. The pipeline uniquely integrates endogenous text (time series patterns description) with exogenous real-world news events through a "Generate-then-Filter" paradigm.

Stage 1: Contextual Synthesis Stage. We adopt a parallel generation strategy to synthesize the textual modality:

- Endogenous Text Generation: An LLM Analyzer GPT-4o is employed to interpret the numerical time series. As shown in Figure 7, guided by specific prompts targeting statistical properties (e.g., trend, seasonality, and stationarity), the analyzer converts raw temporal dynamics into structured Endogenous Text descriptions.
- Exogenous News Retrieval: Simultaneously, we extract metadata constraints—specifically Domain, Time Horizon, and Region—to formulate search queries. We utilize a Relevance Retrieval to fetch the relevant news events from the GDELT Database. These raw articles are then summarized by GPT-4o to form concise Exogenous News, providing the necessary background context for the time series. Specific exogenous news summarization prompt is in Figure 8.

Stage 2: Quality Alignment Stage. To ensure the reliability and logical consistency of the synthesized data, the raw generations undergo a rigorous quality control process:

- Logical Consistency Check: A dedicated LLM GPT-4o evaluates the alignment between the Endogenous Text and Exogenous News. This step filters out hallucinations or irrelevant pairings by verifying, for example, that a significant market dip is explained by a corresponding negative news event rather than a positive one. Specific logical consistency filtering prompt is in Figure 9.
- Ensemble Quality Evaluation: To mitigate the bias inherent in single-model evaluation, the unified text is scrutinized by a heterogeneous ensemble of LLM judges. We employ a consensus-based filtering mechanism, where only samples achieving high aggregate scores on factual plausibility and semantic clarity are incorporated into the final dataset.

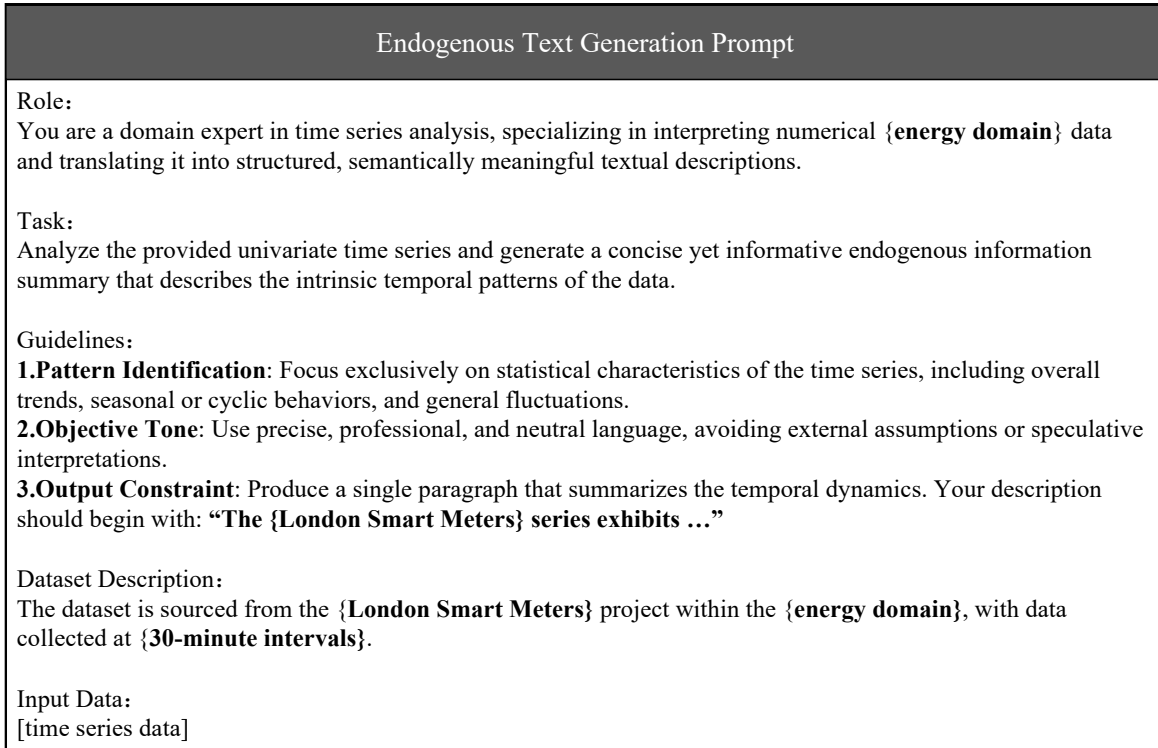


Figure 7. The prompt is designed for generating endogenous descriptions of the London Smart Meters dataset.

**Exogenous News Summarization Prompt**

**Role:**  
You are an expert Data Scientist specializing in time series analysis and macroeconomic forecasting. Your goal is to convert fragmented news headlines into a structured "exogenous information summary".

**Task:**  
Analyze the provided list of news titles and synthesize them into a single, cohesive summary of the external environment.

**Guidelines:**

- Denoising:** Ignore trivial, entertainment, or irrelevant news. Focus on events that could impact economic, social, or environmental variables (e.g., policy changes, extreme weather, strikes, energy crises, or major holidays).
- Synthesis:** If multiple titles refer to the same event, merge them into a single comprehensive description.
- Objective Tone:** Use professional and neutral language. Avoid emotional bias.
- Output Constraint:** Provide ONLY the "Exogenous Information Summary".

**Input Data:**  
[Paste your list of news titles here]

*Figure 8.* The prompt is designed for summarizing the relevant exogenous news.

**Logical Consistency Filtering Prompt**

**Role:**  
You are an expert Time Series Analyst and Logic Auditor. Your task is to rigorously evaluate the causal plausibility and logical consistency between endogenous time series patterns description and exogenous news summary.

**Task:**  
You will be provided with two text inputs: Endogenous Description: A textual description of the time series' data patterns (e.g., trends, seasonality). Exogenous News Summary: A summary of real-world events occurring during the same time of the domain. **Your Goal:** Determine if the Exogenous News logically explains or aligns with the Endogenous Description.

**Guidelines:**

- Directional Alignment Check:** Ensure the news sentiment aligns with the data trajectory: associate rises with positive factors (growth/holidays), declines with negative shocks (crises/outages), and stability with the absence of disruptive events.
- Magnitude Consistency:** A minor data fluctuation should not be paired with a catastrophic global event, and a massive anomaly should not be explained by trivial news.
- Reject Contradictions:** If the news explicitly contradicts the physical reality of the data (e.g., "Electricity usage dropped to zero" vs. "Heatwave causes record power demand"), mark as Inconsistent.

**Input Data:**  
Endogenous Description: [endogenous\_description]  
Exogenous News Summary: [exogenous\_summary]

**Output Format:**  
"consistency\_score": An integer from 1 (Complete Contradiction) to 5 (Perfect Alignment).  
"is\_consistent": Boolean (true if score  $\geq 3$ , else false).

*Figure 9.* The prompt is designed for judgment logical consistency for the endogenous description and exogenous news.

### A.3. Evaluation Dataset

To evaluate HORAI in a multi-task setting, we employ widely used benchmark datasets for both forecasting and anomaly detection. 1) Forecasting: As shown in Table 4, experiments are conducted on TimeMMD (Liu et al., 2024a) and additional datasets (Dong et al., 2024), covering diverse domains such as Agriculture, Climate, Energy, Environment, Social Good, Traffic, EWJ, KR, and MDT. 2) Anomaly Detection: We evaluate HORAI on five datasets—Weather, Energy, KR, EWJ, and MDT—with anomaly ratios ranging from 5.81% to 17.23%. Detailed statistics are provided in Table 5.

Table 4. The statistics of evaluation datasets for the forecasting task.

Tasks	Dataset	Variate	Frequency	Dataset Size	Timespan
Forecasting	Agriculture	1	Monthly	496	1983-2024
	Climate	5	Monthly	496	1983-2024
	Energy	9	Weekly	1479	1996-2024
	Environment	4	Daily	11102	1982-2023
	Social Good	1	Monthly	900	1950-2024
	Traffic	1	Monthly	531	1980-2024
	EWJ	1	Daily	2658	2009-2020
	KR	1	Daily	2655	2009-2020
	MDT	1	Daily	2732	2009-2020

Table 5. The statistics of evaluation datasets for the anomaly detection task.

Tasks	Dataset	Anomaly Ratio	Frequency	Dataset Description
Detection	Weather	17.10%	Monthly	Temperature and humidity information collected from government websites.
	Energy	17.23%	Weekly	The dataset records weekly U.S. gasoline prices (dollars per gallon).
	KR	6.21%	Daily	The dataset is collected from Yahoo, NASDAQ finance websites.
	MDT	11.17%	Monthly	The dataset is collected from Yahoo, NASDAQ finance websites.
	EWJ	9.96%	Daily	The dataset is collected from Yahoo, NASDAQ finance websites.

## B. Baselines

We categorize the baselines into three groups: *Time Series Foundation Models*, *Multimodal Time-Series-Specific Models*, and *Unimodal Time-Series-Specific Models*. Time Series Foundation Models are pre-trained on large-scale, cross-domain unimodal time series data, enabling direct inference on downstream tasks and demonstrating generalization capabilities. In contrast, Time-Series-Specific Models require training on each downstream dataset and can be further divided by input type. Multimodal Time-Series-Specific Models leverage additional modalities, such as text or images, or reuse LLM representations to enhance time series understanding. Unimodal Time-Series-Specific Models, on the other hand, design tailored modules to exploit the inherent characteristics of time series data.

### B.1. Time Series Foundation Models

- ChatTime (Wang et al., 2025a) proposes a unified multimodal time series foundation model that tokenizes both numerical sequences and text prompts into a shared vocabulary, enabling forecasting and question answering tasks with a single generative language-model backbone.
- Sundial (Liu et al., 2025) proposes a TimeFlow Loss that predicts the distribution of the next patch, enabling Transformer training without discrete tokenization and supporting probabilistic forecasting.
- VisionTS (Chen et al., 2024a) converts time series data into image form and uses visual mask autoencoders for unsupervised feature learning.

- ROSE (Wang et al., 2025b) combines frequency decomposition with time-series registers to jointly learn both domain-invariant and domain-specific representations, facilitating knowledge transfer to downstream tasks.
- Timer (Liu et al., 2024c) adopts a decoder-only architecture employing autoregressive modeling for generative pre-training.
- MOIRAI (Woo et al., 2024) introduces multi-scale patch projections to model diverse patterns and an any-variate attention mechanism that allows flexible handling of time series with arbitrary dimensionality.
- DADA (Shentu et al., 2025) leverages adaptive bottleneck and dual-adversarial decoding to enable robust zero-shot anomaly detection across diverse domains.
- UniTS (Gao et al., 2024) proposes a novel unified network backbone for classification, forecasting, and anomaly detection.

## B.2. Multimodal Time-Series-Specific Models

- GPT4MTS (Jia et al., 2024) propose a prompt tuning-based LLM for time series forecasting with multimodal input.
- TATS (Li et al., 2025) propose a plug-and-play multimodal time series forecasting framework, which transforms text representations into auxiliary variables.
- GPT4TS (Zhou et al., 2023) fine-tunes the limited parameters of LLM, demonstrating competitive performance by transferring knowledge from large-scale pre-training text data.
- LLMMixer (Kowsher et al., 2024) adapts LLMs for time series forecasting by breaking down the data into different time scales.
- TimeVLM (Zhong et al., 2025) leverages pre-trained VLMs to enhance time series forecasting by unifying temporal, visual, and textual information.

## B.3. Unimodal Time-Series-Specific Models

- TimesNet (Wu et al., 2023) transforms the 1D time series into a set of 2D tensors based on multiple periods to handle the multi-periodicity of the time series.
- DCdetector (Yang et al., 2023) leverages dual-attention contrastive representation learning, extracting normal feature representations through self-supervised learning and dual-attention mechanisms.
- Anomaly Transformer (Xu et al., 2022) leverages a self-attention mechanism to capture both short- and long-term dependencies in time series, and detects anomalies by analyzing differences in association matrices.
- PatchTST (Nie et al., 2023) segments time series into subseries-level patches that serve as input tokens to the Transformer and applies the channel-independence strategy for training on multivariate time series.
- HBOS (Goldstein & Dengel, 2012) is a fast unsupervised anomaly detection method based on histogram density estimation.
- IForest (Liu et al., 2008) detects anomalies by recursively partitioning data to isolate outliers, rather than modeling normal behavior.
- PCA (Shyu et al., 2003) detects anomalies by measuring deviations in the principal component space, assuming outliers lie far from the normal distribution.

## C. Experiment Setting

During pre-training, HORAI is optimized using the Adam optimizer with an initial learning rate of 0.0005 and trained for 20 epochs, with early stopping applied using a patience of 10 epochs. The batch size is set to 2048, the input time series length to 576, and the patch size to 48. The Time-Frequency Decoder is configured with 6 layers, the model dimension  $D_{model}$  is set to 768, and the ratio parameter  $\alpha$  for high- and low-frequency decomposition is fixed at 0.05. All experiments are implemented in PyTorch, and pre-training is conducted on four NVIDIA Tesla A800 80GB GPUs.

For forecasting, To ensure fairness, we remove the drop-last strategy for HORAI and all baselines, since using it would result in inconsistent numbers of test samples across different batch sizes (Qiu et al., 2024). For each dataset, we evaluate four prediction horizons for both HORAI and the baselines. Specifically, Agriculture, Climate, Social Good, Traffic, EWJ, KR, and MDT are evaluated with horizons {6, 8, 10, 12}, Environment with {48, 96, 192, 336}, and Energy with {12, 24, 36, 48}.

## D. Discussion with ChatTime

We further provide a clarified discussion comparing ChatTime and HORAI, including the following aspects: (1) **Model perspective**: HORAI is **specifically architected as a multimodal foundation model** integrating time series, images, and text. It leverages modality-specific encoders to extract distinct features and employs a novel frequency-enhanced alignment to fuse these representations from multiple perspectives explicitly. In contrast, ChatTime **adapts general-purpose LLMs** for time series analysis. While leveraging LLMs' inherent reasoning abilities for time series analysis offers generalization, discretizing continuous numerical values into textual tokens results in precision loss, making it challenging to capture time series patterns. (2) **Data perspective**: HORAI is pretrained on a large-scale multimodal dataset incorporating aligned text and images. These modalities capture diverse characterizations of temporal dynamics from multiple perspectives and simultaneously introduce some external context, providing relevant supervision that improves generalization. However, ChatTime relies only on simple prompts such as "Please predict the following sequence," which offer limited text regarding the specific time series characteristics.

## E. Model Analysis

### E.1. Sensitivity analysis

We conduct sensitivity experiments on two key parameters: the frequency threshold  $\alpha$  and the number of selected experts  $K$ . As shown in the Table 6, setting  $\alpha$  to 0.05 achieves the best prediction performance. This value distinctly partitions low-frequency from mid-to-high-frequency features, facilitating optimal alignment with text and image modalities. Conversely, a larger  $\alpha$  forces excessive information into high-frequency components, thereby amplifying noise-like patterns; whereas an overly small  $\alpha$  introduces redundant low-frequency information, which disrupts the alignment between image and time series representations. As shown in Table 7, selecting the Top-2 or Top-3 experts yields superior performance. Activating all experts tends to introduce redundancy from irrelevant experts, thereby diluting the model's generalization. Whereas selecting only a single expert limits the representational capacity, preventing the model from modeling diverse patterns.

Table 6. Hyper-parameter sensitivity analysis about the frequency threshold  $\alpha$ .

	$\alpha = 0.01$	$\alpha = 0.05$	$\alpha = 0.25$	$\alpha = 0.5$
Metrics	MSE	MSE	MSE	MSE
Agriculture	0.210	<b>0.201</b>	0.225	0.247
Climate	0.868	<b>0.857</b>	1.054	1.200
Energy	0.228	<b>0.208</b>	0.284	0.266
Environment	0.315	<b>0.309</b>	0.332	0.333

### E.2. Ablation Analysis on Specific Modalities and Alignment Strategies

We perform ablation studies to evaluate the contributions of individual modalities (text, image) and the efficacy of our frequency-based alignment strategy. Specifically, we analyze four settings: 1) only text and time series; 2) only image and time series ; 3) text, image, and time series without frequency-based alignment (w/o Freq-Align); and 4) swapping

Table 7. Hyper-parameter sensitivity analysis about the number of selected experts  $K$ .

Metrics	K=1	K=2	K=3	K=4
Agriculture	0.227	<b>0.201</b>	0.206	0.220
Climate	1.048	<b>0.857</b>	0.880	0.891
Energy	0.217	0.208	<b>0.200</b>	0.215
Environment	0.321	<b>0.309</b>	0.316	0.326

modalities by fusing low-frequency time series with images and mid-to-high frequency time series with text (Modality Exchange). As shown in Table 8, both visual and textual modalities contribute to performance gains, though their relative impact varies depending on the dataset characteristics. For datasets exhibiting clear long-term trends, such as Agriculture and Energy, the text modality contributes more significantly. Conversely, for datasets dominated by local fluctuations, such as Climate, the image modality proves more critical. Crucially, the significant performance drop observed when removing frequency-based alignment and modality exchange underscores the validity of our design: it confirms that aligning images with mid-to-high frequency components and text with low-frequency components is the effective strategy.

Table 8. Ablation analysis about each modality.

	HORAI		Text + Time Series		Image + Time Series		W/O Freq-Align		Modality Exchange	
Metrics	MSE	MAE	MSE	MAE	MSE	MAE	MSE	MAE	MSE	MAE
Agriculture	<b>0.201</b>	<b>0.309</b>	0.248	0.327	0.275	0.340	0.234	0.324	0.292	0.352
Climate	<b>0.857</b>	<b>0.734</b>	1.102	0.828	0.982	0.797	0.928	0.786	1.321	0.856
Energy	<b>0.208</b>	<b>0.325</b>	0.255	0.372	0.276	0.395	0.248	0.355	0.292	0.402
Environment	<b>0.309</b>	<b>0.393</b>	0.344	0.412	0.320	0.398	0.325	0.396	0.360	0.426

### E.3. Ablation Analysis about Text Encoder and Vision Encoder

To evaluate the model’s performance with different encoders, we conduct additional experiments by replacing both text and visual encoders. By default, HORAI employs Qwen-0.5B and ViT-Base for text and visual modalities, respectively. Considering time and computational constraints, we select encoders with relatively small parameter sizes. Specifically, the text encoders include GPT2-small, LLaMA3-1B, and Qwen2.5-1.5B, while the visual encoder comparison uses Swin Transformer. As shown in the Table 9, for a given text encoder, models with larger parameter sizes tend to perform slightly better, and employing more advanced architectures (e.g., Qwen and LLaMA) generally yields further improvements. In the comparison of visual encoders, ViT and Swin Transformer achieve similar overall forecasting performance.

Table 9. Ablation analysis of different text encoders and image encoders.

	HORAI		GPT2		Llama3-1B		Qwen-1.5B		Swin Trans-Base	
Metrics	MSE	MAE	MSE	MAE	MSE	MAE	MSE	MAE	MSE	MAE
Agriculture	0.201	0.309	0.238	0.325	0.210	0.315	0.204	0.314	<b>0.198</b>	<b>0.302</b>
Climate	0.857	0.734	0.913	0.840	0.851	0.730	<b>0.832</b>	<b>0.715</b>	0.863	0.758
Energy	0.208	0.325	0.229	0.348	0.204	0.322	<b>0.202</b>	<b>0.318</b>	0.212	0.336
Environment	0.309	0.393	0.325	0.398	0.310	0.395	0.302	0.390	<b>0.300</b>	<b>0.388</b>

Table 10. Full time series forecasting results of HORAI, time series foundation models, and time-series-specific models.

Type		⌚ Time Series Foundation Models (Zero-Shot)												⌚ Time-Series-Specific-Models (Full-Shot)									
Models		HORAI		ChatTime		VisionTS		ROSE		Timer		MOIRAI		GPT4MTS		TATS		GPT4TS		TimeVLM			
Metric		MSE	MAE	MSE	MAE	MSE	MAE	MSE	MAE	MSE	MAE	MSE	MAE	MSE	MAE	MSE	MAE	MSE	MAE	MSE	MAE	MSE	MAE
Agriculture	6	<b>0.131</b>	0.260	0.243	0.340	0.210	0.289	0.219	0.299	0.168	0.272	0.187	0.342	0.161	0.257	0.140	0.251	<u>0.135</u>	<b>0.242</b>	0.143	<u>0.245</u>		
	8	<b>0.171</b>	0.294	0.349	0.399	0.266	0.323	0.278	0.339	0.243	0.317	0.245	0.391	0.207	0.288	<u>0.187</u>	<b>0.282</b>	0.198	<u>0.284</u>	0.215	0.287		
	10	<b>0.219</b>	0.323	0.390	0.418	0.307	0.348	0.408	0.406	0.328	0.361	0.297	0.423	0.230	0.305	<u>0.244</u>	<u>0.320</u>	0.258	<b>0.313</b>	0.271	0.320		
	12	<b>0.286</b>	0.362	0.497	0.483	0.376	0.386	0.474	0.443	0.415	0.405	0.357	0.455	0.301	<u>0.342</u>	<u>0.290</u>	0.350	0.291	<b>0.338</b>	0.322	0.359		
	avg	<b>0.201</b>	0.309	0.369	0.410	0.290	0.336	0.345	0.372	0.289	0.339	0.272	0.403	0.225	<u>0.298</u>	<u>0.215</u>	0.301	0.220	<b>0.294</b>	0.237	0.302		
Climate	6	<b>0.854</b>	<b>0.736</b>	1.884	1.118	1.316	0.932	1.488	0.993	<u>0.876</u>	<u>0.759</u>	1.624	1.016	1.199	0.895	1.194	0.897	1.207	0.901	1.218	0.907		
	8	<b>0.852</b>	<b>0.733</b>	1.843	1.100	1.312	0.935	1.598	1.031	<u>0.885</u>	<u>0.763</u>	2.148	1.152	1.205	0.899	1.178	0.886	1.191	0.892	1.181	0.914		
	10	<b>0.859</b>	<b>0.734</b>	1.806	1.090	1.302	0.928	1.401	0.967	<u>0.893</u>	<u>0.766</u>	1.983	1.112	1.173	0.885	1.170	0.881	1.169	0.886	1.179	0.880		
	12	<b>0.865</b>	<b>0.736</b>	1.909	1.117	1.297	0.925	1.414	0.957	<u>0.899</u>	<u>0.770</u>	1.929	1.101	1.152	0.876	1.179	0.885	1.171	0.883	1.203	0.896		
	avg	<b>0.857</b>	<b>0.734</b>	1.860	1.106	1.307	0.930	1.475	0.987	<u>0.888</u>	<u>0.764</u>	1.921	1.095	1.182	0.889	1.180	0.887	1.184	0.891	1.195	0.899		
Energy	12	<u>0.105</u>	<u>0.226</u>	<b>0.104</b>	<b>0.222</b>	0.173	0.313	0.268	0.401	0.118	0.236	0.183	0.309	0.111	0.244	0.105	0.232	0.111	0.243	0.114	0.253		
	24	<b>0.189</b>	<b>0.314</b>	<u>0.203</u>	<u>0.321</u>	0.264	0.395	0.363	0.469	0.225	0.336	0.290	0.396	0.232	0.362	0.216	0.344	0.223	0.355	0.227	0.359		
	36	<b>0.248</b>	<b>0.362</b>	<u>0.292</u>	<u>0.396</u>	0.346	0.454	0.413	0.497	0.328	0.403	0.367	0.449	0.308	0.418	0.309	0.418	0.314	0.423	0.309	0.410		
	48	<b>0.292</b>	<b>0.399</b>	0.389	0.470	0.434	0.516	0.501	0.549	0.424	<u>0.460</u>	0.457	0.515	0.398	0.496	<u>0.391</u>	0.480	0.393	0.484	0.390	0.475		
	avg	<b>0.208</b>	<b>0.325</b>	0.247	<u>0.352</u>	0.304	0.420	0.386	0.479	0.274	0.359	0.324	0.417	0.262	0.380	0.255	0.368	0.260	0.376	0.260	0.374		
Environment	48	<u>0.306</u>	<b>0.379</b>	0.343	0.406	0.345	0.426	0.402	0.459	0.358	0.431	0.352	0.404	0.315	0.400	0.307	0.389	0.320	0.396	<b>0.304</b>	0.387		
	96	<b>0.326</b>	<b>0.396</b>	0.369	0.465	0.370	0.441	0.409	0.465	0.368	0.436	0.370	0.415	0.340	0.401	0.334	0.402	0.340	0.401	<u>0.327</u>	<u>0.405</u>		
	192	<b>0.306</b>	<b>0.395</b>	0.377	0.474	0.360	0.442	0.389	0.452	0.351	0.427	0.350	0.402	0.336	0.411	0.332	<u>0.401</u>	0.330	0.391	<u>0.328</u>	0.403		
	336	<b>0.298</b>	<u>0.403</u>	0.372	0.478	0.340	0.436	0.369	0.447	0.326	0.418	0.332	0.390	0.299	0.390	0.302	0.391	<u>0.300</u>	<b>0.383</b>	0.320	0.395		
	avg	<b>0.309</b>	<b>0.393</b>	0.359	0.456	0.354	0.436	0.392	0.456	0.351	0.428	0.351	0.403	0.323	0.400	0.319	0.396	0.322	<u>0.393</u>	<u>0.319</u>	0.397		
Social Good	6	<b>0.682</b>	0.418	0.988	0.451	0.957	0.543	0.939	0.499	0.845	0.416	0.966	0.522	0.718	0.382	0.753	<b>0.370</b>	<u>0.717</u>	<u>0.374</u>	0.732	0.379		
	8	<b>0.779</b>	0.474	1.044	0.488	1.106	0.605	1.168	0.588	0.938	0.469	1.532	0.653	0.942	0.505	0.875	<b>0.409</b>	<u>0.855</u>	0.459	0.822	<u>0.427</u>		
	10	<b>0.869</b>	0.528	1.098	0.519	1.164	0.636	1.187	0.595	1.018	0.515	1.551	0.691	0.929	<b>0.446</b>	0.991	<u>0.459</u>	0.930	0.463	<u>0.916</u>	0.465		
	12	<b>0.948</b>	0.569	1.149	0.554	1.278	0.688	1.272	0.642	1.094	0.557	1.671	0.736	1.093	<b>0.470</b>	1.053	<u>0.474</u>	1.167	0.608	<u>1.005</u>	0.505		
	avg	<b>0.819</b>	0.497	1.069	0.503	1.126	0.618	1.141	0.581	0.974	0.489	1.430	0.651	0.920	0.451	0.918	<b>0.428</b>	0.917	0.476	0.868	0.444		
Traffic	6	<b>0.163</b>	<u>0.240</u>	0.609	0.623	0.275	0.411	0.331	0.449	0.167	0.267	0.349	0.448	0.192	0.264	<u>0.164</u>	<b>0.226</b>	0.199	0.278	0.210	0.316		
	8	<u>0.166</u>	<u>0.245</u>	0.626	0.636	0.282	0.410	0.365	0.455	0.185	0.287	0.461	0.499	0.195	0.256	<u>0.178</u>	<b>0.242</b>	0.204	0.262	0.212	0.313		
	10	<b>0.164</b>	<u>0.246</u>	0.572	0.592	0.286	0.406	0.326	0.443	0.196	0.299	0.414	0.466	0.204	0.257	<u>0.185</u>	<b>0.243</b>	0.210	0.264	0.222	0.328		
	12	<b>0.165</b>	<u>0.247</u>	0.579	0.592	0.282	0.402	0.342	0.458	0.202	0.307	0.400	0.458	0.218	0.268	<u>0.189</u>	<b>0.242</b>	0.211	0.260	0.222	0.322		
	avg	<b>0.165</b>	<u>0.244</u>	0.596	0.610	0.281	0.407	0.341	0.451	0.188	0.290	0.406	0.468	0.203	0.261	<u>0.179</u>	<b>0.238</b>	0.206	0.266	0.216	0.319		
EWJ	6	<b>0.548</b>	0.528	0.808	0.612	0.583	0.560	0.634	0.581	0.643	0.573	0.751	0.623	0.579	0.531	0.550	0.525	<u>0.550</u>	<u>0.523</u>	0.552	<b>0.521</b>		
	8	<b>0.581</b>	<b>0.537</b>	0.880	0.641	0.629	0.580	0.729	0.626	0.685	0.591	1.017	0.714	0.608	0.540	0.611	0.544	<u>0.597</u>	<u>0.538</u>	0.599	0.541		
	10	<b>0.604</b>	<b>0.550</b>	0.920	0.652	0.665	0.591	0.716	0.599	0.716	0.604	0.982	0.705	0.644	0.559	<u>0.627</u>	<b>0.551</b>	0.632	0.551	0.629	0.554		
	12	<b>0.623</b>	<b>0.558</b>	0.940	0.659	0.701	0.607	0.746	0.613	0.740	0.614	0.997	0.709	0.673	0.566	0.661	0.563	<u>0.649</u>	<u>0.560</u>	0.657	0.562		
	avg	<b>0.589</b>	<b>0.543</b>	0.887	0.641	0.645	0.584	0.706	0.605	0.696	0.595	0.937	0.688	0.626	0.549	0.612	0.546	<u>0.607</u>	<b>0.543</b>	0.609	0.544		
KR	6	<b>0.533</b>	<b>0.435</b>	0.528	0.436	0.628	0.503	0.687	0.521	0.530	0.453	0.793	0.567	0.528	0.442	0.542	<u>0.426</u>	<u>0.539</u>	0.435	0.550	0.437		
	8	<b>0.549</b>	<b>0.446</b>	0.564	0.452	0.674	0.524	0.798	0.572	0.547	0.461	1.077	0.650	0.564	<u>0.452</u>	0.569	0.446	0.573	0.444	0.580	0.451		
	10	0.561	<b>0.454</b>	0.570	0.459	0.685	0.526	0.727	0.530	<b>0.559</b>	0.468	1.063	0.649	0.566	0.455	0.600	0.462	0.594	<u>0.452</u>	0.601	0.463		
	12	<b>0.562</b>	<u>0.458</u>	0.598	0.473	0.698	0.535	0.750	0.547	0.560	0.472	1.038	0.649	0.562	<b>0.453</b>	0.602	0.461	0.604	0.459	0.606	0.467		
	avg	<b>0.551</b>	<b>0.448</b>	0.565	0.455	0.671	0.522	0.741	0.542	0.549	0.463	0.992	0.629	0.555	<u>0.450</u>	0.578	0.449	0.578	0.448	0.584	0.454		
MDT	6	<b>0.361</b>	0.426	0.466	0.455	0.412	0.471	0.426	0.476	0.366	0.437	0.494	0.521	<b>0.369</b>	0.436	0.423	<u>0.373</u>	<b>0.422</b>	0.369	<u>0.423</u>			
	8	<b>0.372</b>	<b>0.433</b>	0.474	0.473	0.431	0.486	0.483</td															

Table 11. Time series anomaly detection results under zero-shot and full-shot settings with multiple metrics. The best results are in **bold**, and the second-best results are underlined.

Type	Metric	⌚ Time Series Foundation Models (Zero-Shot)				⌚ Time-Series-Specific-Models (Full-Shot)									
		HORAI	DADA	Timer	UniTS	GPT4TS	LLMMixer	TimesNet	DCdetector	A.T.	PatchTST	HBOS	IForest	PCA	
EWJ	Aff-F1	<b>82.54</b>	81.26	78.06	77.61	76.65	66.86	<u>81.82</u>	48.10	59.03	75.82	71.03	67.55	51.06	
	F1	<b>56.28</b>	49.33	41.21	39.18	48.33	18.95	<u>49.37</u>	17.09	14.39	45.39	44.80	41.67	18.68	
	Range-AUC-ROC	<b>79.84</b>	68.44	64.71	67.15	55.57	41.75	<u>74.22</u>	45.69	27.50	69.26	61.02	57.94	43.78	
	Range-AUC-PR	<b>43.33</b>	41.61	30.67	44.31	32.83	12.36	<u>41.84</u>	12.52	9.01	33.37	46.37	34.77	16.49	
	AUC-PR	51.97	<b>55.24</b>	44.01	50.33	46.75	18.81	<u>54.99</u>	10.88	8.97	47.91	25.24	24.16	10.99	
	AUC-ROC	<b>86.95</b>	79.11	76.15	79.87	75.58	57.69	<u>82.39</u>	53.40	43.81	78.53	71.82	69.20	54.35	
	VUS-ROC	<b>82.78</b>	71.79	67.72	73.91	67.95	52.79	<u>75.76</u>	47.10	31.75	71.96	62.07	59.24	45.26	
	VUS-PR	<b>48.27</b>	43.36	33.17	39.32	35.63	15.13	<u>43.15</u>	15.37	10.85	36.08	41.19	37.81	19.38	
MDT	Aff-F1	<b>80.66</b>	77.99	78.51	75.57	80.81	67.65	<u>80.08</u>	47.33	66.12	79.47	52.33	53.74	54.66	
	F1	<b>59.36</b>	53.70	48.39	51.70	49.14	27.71	<u>54.88</u>	19.54	25.46	49.40	43.84	38.10	20.75	
	Range-AUC-ROC	<b>86.59</b>	63.94	58.98	58.78	59.00	42.44	<u>77.01</u>	43.65	41.41	75.61	54.86	53.22	41.90	
	Range-AUC-PR	<b>51.11</b>	44.63	37.54	36.14	42.48	15.30	48.60	13.30	13.20	13.11	43.16	33.63	19.53	
	AUC-PR	61.98	<u>63.03</u>	55.86	53.44	60.40	19.86	<b>65.57</b>	11.59	15.29	54.11	28.66	22.41	12.29	
	AUC-ROC	<b>91.22</b>	79.04	75.65	73.19	74.79	60.30	<u>86.67</u>	53.82	56.44	84.55	60.26	63.92	54.51	
	VUS-ROC	<b>86.82</b>	66.76	60.28	58.67	62.30	46.80	<u>83.40</u>	45.02	44.53	77.69	55.30	54.02	44.09	
	VUS-PR	<b>56.88</b>	46.81	38.38	37.61	44.81	15.21	<u>52.13</u>	15.72	15.93	41.67	44.77	35.32	22.93	
KR	Aff-F1	<b>85.44</b>	84.22	89.55	82.24	79.56	71.80	85.47	61.94	70.99	79.52	64.78	69.38	58.11	
	F1	<b>71.89</b>	49.48	58.04	30.23	74.01	20.25	58.14	11.98	11.10	36.64	<u>60.71</u>	53.97	22.76	
	Range-AUC-ROC	<b>86.16</b>	69.91	74.61	71.29	65.15	49.01	<u>78.29</u>	41.75	40.18	72.72	61.80	61.10	51.01	
	Range-AUC-PR	<b>59.64</b>	46.95	51.59	<b>40.75</b>	37.53	13.25	<u>52.83</u>	6.04	7.44	35.22	51.69	43.07	18.99	
	AUC-PR	<b>72.91</b>	63.55	66.72	55.39	56.78	28.19	<u>67.47</u>	8.10	7.01	53.60	41.09	32.21	10.18	
	AUC-ROC	<b>96.38</b>	79.53	66.72	80.95	78.30	65.77	<u>85.88</u>	52.97	51.25	82.15	75.16	74.45	63.58	
	VUS-ROC	<b>93.54</b>	70.82	75.99	73.93	67.81	47.06	<u>79.00</u>	43.04	41.97	74.65	58.77	60.70	47.51	
	VUS-PR	<b>60.76</b>	45.90	51.41	43.32	38.23	19.10	<u>51.60</u>	8.49	7.94	36.18	54.17	43.31	24.19	
Energy	Aff-F1	<b>71.37</b>	64.38	60.20	63.84	<u>66.37</u>	65.85	66.00	47.07	43.39	66.85	55.85	62.03	57.65	
	F1	<b>37.71</b>	31.54	31.71	31.66	33.22	33.08	33.95	12.63	12.05	34.81	<u>34.83</u>	34.39	35.12	
	Range-AUC-ROC	<b>62.93</b>	55.78	46.82	52.12	53.54	55.25	<u>61.56</u>	45.39	31.52	61.39	51.06	52.64	52.64	
	Range-AUC-PR	33.24	33.47	28.81	30.70	31.10	30.59	<u>38.17</u>	21.77	19.24	35.25	42.14	45.19	<b>43.89</b>	
	AUC-PR	<u>39.82</u>	37.81	38.05	27.51	33.75	32.85	<b>42.05</b>	17.69	14.02	34.25	21.55	21.17	21.69	
	AUC-ROC	<b>68.44</b>	62.33	60.54	63.38	66.54	61.31	<u>68.36</u>	48.75	38.68	66.70	60.80	60.32	61.14	
	VUS-ROC	<b>62.42</b>	54.37	46.03	51.15	53.10	53.04	<u>59.47</u>	45.93	31.56	58.31	51.50	53.61	53.07	
	VUS-PR	35.24	34.18	29.46	31.04	31.68	30.35	38.61	22.57	19.69	34.41	<u>42.57</u>	<b>46.03</b>	44.30	
Weather	Aff-F1	<b>80.84</b>	69.01	75.46	76.17	72.56	73.68	<u>80.58</u>	42.80	49.22	77.17	47.70	54.06	64.91	
	F1	47.44	35.29	46.42	<u>50.00</u>	40.16	43.13	<b>51.58</b>	11.14	15.59	49.60	42.94	49.21	40.41	
	Range-AUC-ROC	<b>80.61</b>	61.95	73.37	75.55	71.43	72.54	<b>83.11</b>	45.41	43.11	80.47	54.12	56.69	57.80	
	Range-AUC-PR	<b>50.88</b>	29.86	43.20	44.31	41.37	43.40	<u>50.58</u>	18.06	18.85	49.81	46.37	49.65	47.47	
	AUC-PR	49.16	29.80	48.87	<u>49.91</u>	44.12	49.71	47.56	17.08	16.71	<b>53.39</b>	31.16	35.44	25.02	
	AUC-ROC	<b>81.49</b>	66.37	80.86	81.22	74.47	79.60	<u>81.10</u>	47.90	47.11	82.02	64.47	67.81	67.71	
	VUS-ROC	<u>80.40</u>	61.03	73.22	75.08	70.03	71.71	<b>81.91</b>	45.56	43.32	79.97	54.16	56.45	57.38	
	VUS-PR	<b>50.76</b>	30.00	43.21	44.35	41.30	43.47	50.09	18.33	19.17	<u>50.13</u>	46.58	49.66	47.13	
1 <sup>st</sup> Count		<b>31</b>	1	0	0	0	0	<u>5</u>	0	0	1	0	1	1	